Partially coherent sources with controllable radial and azimuthal periodicity

MEILAN LUO[1, 2, *], **MATIAS KOIVUROVA**[3, 4], **JARI TURUNEN**[2]

[1] *Department of Physics and Synergetic Innovation Center for Quantum Effects and Applications, Hunan Normal University, Changsha, Hunan 410081, China*
[2] *University of Eastern Finland, Institute of Photonics, P.O. Box 111, FI-80101 Joensuu, Finland*
[3] *Tampere Institute for Advanced Study, Tampere University, 33100 Tampere, Finland*
[4] *Faculty of Engineering and Natural Sciences, Tampere University, 33720 Tampere, Finland*
[*] *mlluo@hunnu.edu.cn*

Abstract: We introduce a class of partially coherent sources, which are capable of producing beams with radially quasi-periodic and azimuthally fully periodic intensity profiles. The physical properties of the source, as well as the propagation of the intensity distribution and the complex degree of spatial coherence of the ensuing beams are investigated and interpreted. It is shown that the shape and symmetry of the intensity and the complex degree of spatial coherence are generally adjustable and modulated by the parameters related to the beam source. Moreover, the periodic changes of intensity arise from the discontinuity of the phase. The results provide a method for synthesizing fields with peculiar periodic intensity distributions in polar coordinates.

1. Introduction

Over the past few decades, there has been an increased interest towards the properties of partially coherent beams, since they hold great potential for a variety of practical applications, such as optical trapping and manipulation [1], optical coherence tomography [2], and optical communication [3]. Aside from the analytically simple Gaussian Schell-model (GSM) beams [4], construction of light fields with non-GSM correlation functions has become one of the main targets of modern coherence research. This is due to the peculiar correlation induced effects, which may also shape the intensity pattern of a light beam when the complex degree of spatial coherence (DOC) is chosen properly. A superposition integral method introduced by Gori et al. [5, 6] allows for devising genuine spatial correlation functions both for scalar and electromagnetic beam sources. Following this method, many partially coherent fields have recently been introduced, including nonuniformly correlated, ring shaped, azimuthally dependent beams, twisted Laguerre-GSM correlated beams, as well as self-splitting pulses [7–11].

Several recent studies have shown that certain beam arrays or optical lattices can be achieved by constructing periodic source-plane DOCs. Such sources have found useful applications ranging from optical rerouting of microflow-driven materials to periodic pinning of viscously damped particles [12, 13]. To date, common examples of partially coherent spatially periodic beam arrays includes rectangular GSM array beams [14, 15] and annular vortex beam arrays [16, 17]. However, little attention has been paid to arrays with more complex periodicity. Therefore, constructing beam arrays with adjustable radial and azimuthal periodicity is of practical significance, since it could offer more opportunities to discover the full potential of optical trapping and guiding of molecules or nano/micro particles. Besides the symmetric instances of array beams, where only the magnitude of DOC is modelled, some efforts have been devoted to the construction of asymmetric coherence gratings [18].

In addition, common to all these array beams is the presence of index of summation. The GSM array beam, for instance, usually requires two summation indices. However, evaluation of infinite series reduces, in general, the efficiency of simulation. In this paper, we introduce a class

of partially coherent beam sources, without a summation index, whose DOC is modulated by a Bessel function and an azimuthally periodic function. Such a beam takes on a quasi radially and azimuthally periodic (RAP) intensity pattern in the far field, a significant difference to previous beam models whose intensity patterns are mostly periodic in Cartesian coordinates. We study the propagation properties of the beam in the Fresnel region and in the far field. The results show that the periodicity and symmetry of the intensity produced by such a beam can be modulated by parameters relevant to the beam source, such as the order of the Bessel function and global coherence. The unique intensity patterns that can be dynamically controllable may match the requirements of particular applications.

2. Partially coherent source model with quasi RAP correlations

We consider statistically stationary, spatially partially coherent scalar fields at a frequency ω, which we leave implicit for brevity. The second-order correlation properties of the fields at two spatial positions $\boldsymbol{\rho}_1' = (x_1', y_1')$ and $\boldsymbol{\rho}_2' = (x_2', y_2')$ at the source plane $z = 0$ can be characterized by the cross-spectral density (CSD) function [19]

$$W^{(0)}(\boldsymbol{\rho}_1', \boldsymbol{\rho}_2') = \langle E^*(\boldsymbol{\rho}_1') E(\boldsymbol{\rho}_2') \rangle, \tag{1}$$

where $E(\boldsymbol{\rho}')$ is the electric field, the asterisk denotes complex conjugation, and the angle brackets stand for ensemble averaging. The sufficient condition that ensures the non-negative definiteness of the CSD can be written in the form [5]

$$W^{(0)}(\boldsymbol{\rho}_1', \boldsymbol{\rho}_2') = \int_{-\infty}^{\infty} p(\boldsymbol{v}) H^{(0)*}(\boldsymbol{\rho}_1', \boldsymbol{v}) H^{(0)}(\boldsymbol{\rho}_2', \boldsymbol{v}) \mathrm{d}^2\boldsymbol{v}, \tag{2}$$

where $p(\boldsymbol{v})$ is a real, non-negative, and Fourier transformable function of a vector variable $\boldsymbol{v} = (v_x, v_y)$, and $H^{(0)}(\boldsymbol{\rho}', \boldsymbol{v})$ represents the kernel of an arbitrary linear transformation. If we choose a Fourier kernel

$$H^{(0)}(\boldsymbol{\rho}', \boldsymbol{v}) = H^{(0)}(\boldsymbol{\rho}') \exp\left(-i2\pi \boldsymbol{\rho}' \cdot \boldsymbol{v}\right), \tag{3}$$

the CSD in Eq. (2) factorizes into the Schell-model [20] form

$$W^{(0)}(\boldsymbol{\rho}_1', \boldsymbol{\rho}_2') = H^{(0)*}(\boldsymbol{\rho}_1') H^{(0)}(\boldsymbol{\rho}_2') f(\Delta\boldsymbol{\rho}'), \tag{4}$$

where $\Delta\boldsymbol{\rho}' = \boldsymbol{\rho}_2' - \boldsymbol{\rho}_1'$ and

$$f(\Delta\boldsymbol{\rho}') = \int_{-\infty}^{\infty} p(\boldsymbol{v}) \exp\left(-i2\pi \Delta\boldsymbol{\rho}' \cdot \boldsymbol{v}\right) \mathrm{d}^2\boldsymbol{v}, \tag{5}$$

is the inverse Fourier transform of the profile function $p(\boldsymbol{v})$.

In what follows, we specifically assume that the spatial part of the Fourier kernel is a real-valued Gaussian function characterized by a width parameter w_0, i.e.,

$$H^{(0)}(\boldsymbol{\rho}') = H_0 \exp\left(-\frac{\boldsymbol{\rho}'^2}{w_0^2}\right). \tag{6}$$

The spectral density of the field can then be written as

$$S^{(0)}(\boldsymbol{\rho}') = W^{(0)}(\boldsymbol{\rho}', \boldsymbol{\rho}') = S_0 \exp\left(-\frac{2\boldsymbol{\rho}'^2}{w_0^2}\right), \tag{7}$$

where $S_0 = H_0^2 f(0)$ and the parameter w_0 represents the waist width of the beam source. The complex spatial DOC at the source plane takes the form

$$\mu^{(0)}(\boldsymbol{\rho}_1', \boldsymbol{\rho}_2') = \frac{W^{(0)}(\boldsymbol{\rho}_1', \boldsymbol{\rho}_2')}{\sqrt{S^{(0)}(\boldsymbol{\rho}_1') S^{(0)}(\boldsymbol{\rho}_2')}} = \frac{f(\Delta\boldsymbol{\rho}')}{f(0)}, \tag{8}$$

which depends only on the coordinate difference, i.e., $\mu^{(0)}(\boldsymbol{\rho}_1', \boldsymbol{\rho}_2') = \mu^{(0)}(\Delta\boldsymbol{\rho}')$, since $H^{(0)}(\boldsymbol{\rho}')$ is real-valued.

To generate a quasi RAP beam, it is convenient to express the spatial-frequency vector $\boldsymbol{\nu}$ in polar coordinates (ν, ϕ) defined by writing $\nu_x = \nu \cos\phi$, $\nu_y = \nu \sin\phi$. Here we assume that the function $p(\boldsymbol{\nu})$ has the particular form

$$p(\nu, \phi) = 2\pi\sigma_0^2 p_m \exp\left(-2\pi^2\sigma_0^2\nu^2\right) \left[1 \pm J_m(2\pi r_0 \nu)\cos(m\phi)\right], \tag{9}$$

where σ_0 and r_0 are real constants with values $\sigma_0 > 0$ and $r_0 \geq 0$, and $J_m(z)$ denotes the Bessel function of the first kind and order m. The constant p_m is chosen as

$$p_m = \begin{cases} \left\{1 \pm \exp\left[-r_0^2/(2\sigma_0^2)\right]\right\}^{-1} & \text{when } m = 0 \\ 1 & \text{when } m \neq 0 \end{cases} \tag{10}$$

to ensure that $f(0) = 1$ in Eq. (8). Since $J_{-m}(z) = (-1)^m J_m(z)$, we need to consider only non-negative values of m.

It is now convenient to introduce polar spatial-difference coordinates $\Delta\boldsymbol{\rho}' = (\Delta\rho', \Delta\varphi')$ by writing $\Delta x' = \Delta\rho' \cos\Delta\varphi'$, $\Delta y' = \Delta\rho' \sin\Delta\varphi'$. In what follows, we will consider field properties using two characteristic ratios:

$$q = \sigma_0 / w_0 \tag{11}$$

and

$$r = r_0/\sigma_0 = R/q, \tag{12}$$

where $R = r_0/w_0$ and the ratio q is a measure of the global DOC of the standard GSM beam. Then, on inserting from Eq. (9) into Eq. (5) and making use of Eq. (8), we find by straightforward integration that the source-plane DOC has a rotationally symmetric form (see the Appendix for details of the derivation)

$$\mu^{(0)}(\Delta\rho') = p_m \exp\left(-\frac{\Delta\rho'^2}{2\sigma_0^2}\right)\left[1 + C_m(-i)^m \cos(m\Delta\varphi') \exp\left(-\frac{r^2}{2}\right) I_m\left(\frac{r\Delta\rho'}{\sigma_0}\right)\right]. \tag{13}$$

Here C_m takes values of ± 1 for case of $m = 0$, while $C_m = 1$ for $m > 0$. Moreover, $I_m(z)$ is a modified Bessel function of the first kind and order m. Considering first the case $m = 0$, Eq. (13) reduces to the DOC of a GSM beam when $C_0 = 1$ is chosen and $r_0 \to 0$. On the other hand, if $C_0 = -1$ and we again let $r_0 \to 0$, we have

$$\mu^{(0)}(\Delta\rho') = \exp\left(-\frac{\Delta\rho'^2}{2\sigma_0^2}\right)\left(1 - \frac{\Delta\rho'^2}{2\sigma_0^2}\right). \tag{14}$$

This DOC is positive when $\Delta\rho'/\sigma_0 < \sqrt{2}$ and negative otherwise, therefore having a well-defined central lobe and a single annular side lobe with a maximum value $\left|\mu^{(0)}(\Delta\rho')\right| = 1/\mathrm{e}^2$ at $\Delta\rho'/\sigma_0 = 2$. This solution is recognized as the DOC of a Laguerre–Gauss Schell-model (LGSM) source [8] of order $n = 1$.

For values $m > 0$, if $r = 0$, Eq. (13) reduces to an azimuthally periodic solution

$$\mu^{(0)}(\Delta\rho', \Delta\varphi') = \exp\left(-\frac{\Delta\rho'^2}{2\sigma_0^2}\right)[1 + \cos(m\Delta\varphi')]\,. \tag{15}$$

For values $r > 0$, the presence of index m in both the cosine function and the Bessel function permits simultaneous control of the DOC in both radial and azimuthal directions. We further note that, for odd values of m, the DOC at the source plane is complex, meaning that the intensity pattern in the far field is asymmetric about the origin. For even values of m, the DOC is real, indicating that the far field intensity pattern is symmetric about the origin. These observations follow from basic Fourier optics considerations.

3. Propagation of partially coherent quasi RAP beams

The source described by $W^{(0)}(\boldsymbol{\rho}_1', \boldsymbol{\rho}_2')$, with the spectral density given by Eq. (7) and the DOC defined in Eq. (13), radiates a beamlike field that propagates towards the positive half-space $z > 0$. Within the paraxial approximation, the propagation of the CSD function between two position vectors $\boldsymbol{\rho}_1 = (x_1, y_1)$ and $\boldsymbol{\rho}_2 = (x_2, y_2)$ at any transverse plane is governed by the formula [19]

$$W(\boldsymbol{\rho}_1, \boldsymbol{\rho}_2, z) = \iint_{-\infty}^{\infty} W^{(0)}(\boldsymbol{\rho}_1', \boldsymbol{\rho}_2') G^*(\boldsymbol{\rho}_1 - \boldsymbol{\rho}_1', z) G(\boldsymbol{\rho}_2 - \boldsymbol{\rho}_2', z) \mathrm{d}^2\boldsymbol{\rho}_1' \mathrm{d}^2\boldsymbol{\rho}_2'. \tag{16}$$

Here G is the propagation kernel that can be written as

$$G(\boldsymbol{\rho} - \boldsymbol{\rho}', z) = -\frac{ik}{2\pi z} \exp\left(ik\frac{|\boldsymbol{\rho} - \boldsymbol{\rho}'|^2}{2z}\right), \tag{17}$$

where $k = 2\pi/\lambda$ is the wave number in the half-space $z > 0$, λ being the wavelength. Substituting from Eq. (2) into Eq. (16) and interchanging the order of integration yields

$$W(\boldsymbol{\rho}_1, \boldsymbol{\rho}_2, z) = \int_{-\infty}^{\infty} p(\boldsymbol{v}) H^*(\boldsymbol{\rho}_1, \boldsymbol{v}, z) H(\boldsymbol{\rho}_2, \boldsymbol{v}, z) \mathrm{d}^2\boldsymbol{v}, \tag{18}$$

with a kernel

$$H(\boldsymbol{\rho}, \boldsymbol{v}, z) = \int_{-\infty}^{\infty} H^{(0)}(\boldsymbol{\rho}', \boldsymbol{v}) G(\boldsymbol{\rho} - \boldsymbol{\rho}', z) \mathrm{d}^2\boldsymbol{\rho}'. \tag{19}$$

One can readily see that Eq. (18) has a similar mathematical form as Eq. (2), only the integration kernels are different. Hence, we can use the same treatment as in the derivation of $W^{(0)}(\boldsymbol{\rho}_1', \boldsymbol{\rho}_2')$ to obtain an analytic expression of $W(\boldsymbol{\rho}_1, \boldsymbol{\rho}_2, z)$. Substituting Eqs. (3) and (17) into Eq. (19) and performing the integral, the product of the two kernels becomes

$$\begin{aligned} H^*(\boldsymbol{\rho}_1, \boldsymbol{v}, z) H(\boldsymbol{\rho}_2, \boldsymbol{v}, z) = \frac{k^2}{4z^2|a(z)|^2} \exp\left\{\frac{ik}{2z}\left(\boldsymbol{\rho}_2^2 - \boldsymbol{\rho}_1^2\right) - \frac{k^2}{4z^2}\left[\frac{\boldsymbol{\rho}_1^2}{a(z)} + \frac{\boldsymbol{\rho}_2^2}{a^*(z)}\right]\right\} \\ \times \exp\left\{-\pi^2\left[\frac{1}{a(z)} + \frac{1}{a^*(z)}\right]\boldsymbol{v}^2 - \frac{k\pi}{z}\left[\frac{\boldsymbol{v}\cdot\boldsymbol{\rho}_1}{a(z)} + \frac{\boldsymbol{v}\cdot\boldsymbol{\rho}_2}{a^*(z)}\right]\right\}. \end{aligned} \tag{20}$$

Here we have used a short-hand notation

$$a(z) = 1/w_0^2 + ik/(2z) = (1 + iz_\mathrm{G}/z)/w_0^2, \tag{21}$$

where $z_\mathrm{G} = kw_0^2/2$ is the Rayleigh range of a fully coherent Gaussian beam. On performing the integral in Eq. (18), we may cast the propagated CSD in the explicit form

$$\begin{aligned} W(\boldsymbol{\rho}_1, \boldsymbol{\rho}_2, z) = p_m \frac{w_0^2}{w^2(z)} \exp\left[-\frac{\boldsymbol{\rho}_1^2 + \boldsymbol{\rho}_2^2}{w^2(z)}\right] \exp\left[-\frac{\Delta\boldsymbol{\rho}^2}{2q^2w^2(z)}\right] \\ \times \exp\left[-\frac{ik}{2R(z)}\left(\boldsymbol{\rho}_1^2 - \boldsymbol{\rho}_2^2\right)\right] F(\boldsymbol{\rho}_1, \boldsymbol{\rho}_2, z) \end{aligned} \tag{22}$$

with

$$F(\boldsymbol{\rho}_1, \boldsymbol{\rho}_2, z) = 1 + C_m(-1)^m \cos\left[m f_{12}(\boldsymbol{\rho}_1, \boldsymbol{\rho}_2, z)\right] \times \exp\left[-\frac{r^2}{2}c(z)\right] J_m\left[\frac{kr}{2}\frac{c(z)}{z} g(\boldsymbol{\rho}_1, \boldsymbol{\rho}_2, z)\right]. \tag{23}$$

In Eq. (22), we have made use of the two standard propagation parameters of GSM beams [21], namely the beam width

$$w(z) = w_0[1 + (z/z_\mathrm{R})^2]^{1/2} \tag{24}$$

and the radius of wave front curvature

$$R(z) = z\left[1 + (z_\mathrm{R}/z)^2\right], \tag{25}$$

where

$$z_\mathrm{R} = z_\mathrm{G}\left(1 + q^{-2}\right)^{-1/2} \tag{26}$$

denotes the Rayleigh range of the GSM beam. Additionally, in Eq. (23), we have employed the following shorthand notations:

$$c(z) = \frac{1 + (z/z_\mathrm{G})^2}{1 + (z/z_\mathrm{R})^2}, \tag{27a}$$

$$g(\boldsymbol{\rho}_1, \boldsymbol{\rho}_2, z) = \frac{1}{\sigma_0}\left[\frac{\rho_1^2}{a^2(z)} + \frac{\rho_2^2}{a^{*2}(z)} + \frac{2\rho_1\rho_2\cos\Delta\varphi}{|a(z)|^2}\right]^{1/2}, \tag{27b}$$

$$f_{12}(\boldsymbol{\rho}_1, \boldsymbol{\rho}_2, z) = \arctan\left\{\frac{[\rho_1/a(z)]\sin\varphi_1 + [\rho_2/a^*(z)]\sin\varphi_2}{[\rho_1/a(z)]\cos\varphi_1 + [\rho_2/a^*(z)]\cos\varphi_2}\right\}, \tag{27c}$$

where polar coordinates $\boldsymbol{\rho} = (\rho, \varphi)$ have been used. It immediately follows from Eq. (23) that Eq. (22) reduces to the basic GSM beam when the positive sign is chosen for $m = 0$ and $r_0 = 0$. It can be also seen from Eq. (22) that, apart from common curvature and transverse widening factors, the CSD retains its mathematical form upon propagation in the sense that $F(\boldsymbol{\rho}_1, \boldsymbol{\rho}_2, z)$ contains both cosine and Bessel terms.

Looking at the spatial distribution of the spectral density of the propagated beam by writing $\boldsymbol{\rho}_1 = \boldsymbol{\rho}_2 = \boldsymbol{\rho}$ in Eq. (22) and simplifying, we obtain

$$S(\boldsymbol{\rho}, z) = p_m \frac{w_0^2}{w^2(z)} \exp\left[-\frac{2\boldsymbol{\rho}^2}{w^2(z)}\right] \times \left\{1 + C_m(-1)^m \cos(m\varphi) \exp\left[-\frac{R^2}{2q^2}c(z)\right] J_m\left[\frac{2R}{q\sqrt{1+q^2}} \frac{z/z_\mathrm{R}}{1 + (z/z_\mathrm{R})^2} \frac{\rho}{w_0}\right]\right\}. \tag{28}$$

Compared to conventional partially coherent beams with Cartesian or annular symmetry, Eq. (28) contains a richer variety of intensity profiles, determined by both the azimuthal dependence in the cosine function and the radial dependence in the Bessel function. More precisely, the azimuthal periodicity is given by $2\pi/m$, and the radial spacing is governed by the zeros of the derivative of the Bessel function of mth order. Further, one can find from the argument of the Bessel function in Eq. (28) that the radial periodicity depends on the global coherence parameter q, as well as the propagation distance z, and is inversely proportional to the parameter R. Since the zeros of the derivative of the Bessel function are not equally spaced, the intensity pattern of the beam has quasi radial periodicity.

Let us next consider the behavior of the field in the far zone, $z \gg z_{\mathrm{R}}$. It follows directly from Eqs. (24) and (25) that $w(z) \to w_0 z/z_{\mathrm{R}}$ and $R(z) \to z$ as $z \to \infty$, which give

$$W^{(\infty)}(\boldsymbol{\rho}_1, \boldsymbol{\rho}_2, z) = p_m \frac{z_{\mathrm{R}}^2}{z^2} \exp\left(-\frac{z_{\mathrm{R}}^2}{z^2} \frac{\boldsymbol{\rho}_1^2 + \boldsymbol{\rho}_2^2}{w_0^2}\right) \exp\left(-\frac{z_{\mathrm{R}}^2}{z^2} \frac{\Delta\boldsymbol{\rho}^2}{2q^2 w_0^2}\right) \exp\left[-\frac{ik}{2z}\left(\boldsymbol{\rho}_1^2 - \boldsymbol{\rho}_2^2\right)\right] \times F^{(\infty)}(\boldsymbol{\rho}_1, \boldsymbol{\rho}_2, z). \tag{29}$$

In the far zone we also have the limits $a(z) \to 1/w_0^2$, $c(z) \to 1/(1+q^{-2})$, $g(\boldsymbol{\rho}_1, \boldsymbol{\rho}_2, z) \to w_0^2 |\boldsymbol{\rho}_1 + \boldsymbol{\rho}_2|/\sigma_0$, and $f_{12}(\boldsymbol{\rho}_1, \boldsymbol{\rho}_2, z) \to \arg(\boldsymbol{\rho}_1 + \boldsymbol{\rho}_2)$. We therefore get

$$F^{(\infty)}(\boldsymbol{\rho}_1, \boldsymbol{\rho}_2, z) = 1 + C_m (-1)^m \cos\left[m \arg(\boldsymbol{\rho}_1 + \boldsymbol{\rho}_2)\right] \exp\left[-\frac{R^2}{2(1+q^2)}\right] \times J_m\left(\frac{R}{q\sqrt{1+q^2}} \frac{z_{\mathrm{R}}}{z} \frac{|\boldsymbol{\rho}_1 + \boldsymbol{\rho}_2|}{w_0}\right). \tag{30}$$

Hence, the spectral density in the far zone is given by

$$S^{(\infty)}(\boldsymbol{\rho}, z) = p_m \frac{z_{\mathrm{R}}^2}{z^2} \exp\left(-\frac{z_{\mathrm{R}}^2}{z^2} \frac{2\boldsymbol{\rho}^2}{w_0^2}\right) \times \left\{1 + C_m (-1)^m \cos(m\varphi) \exp\left[-\frac{R^2}{2(1+q^2)}\right] J_m\left(\frac{2R}{q\sqrt{1+q^2}} \frac{z_{\mathrm{R}}}{z} \frac{\rho}{w_0}\right)\right\}. \tag{31}$$

Therefore, the far-zone beam properties become independent on z, as they should, if the spherical phase in Eq. (29) is extracted and we normalize the transverse coordinates to $w_0 z/z_{\mathrm{R}}$.

At this stage it is appropriate to look at certain limiting cases. In the fully coherent limit $q \to \infty$, the intensity profile remains Gaussian at all distances if $m = 0$ and either sign of C_0 is chosen. If $m > 0$, the far-zone spectral density reduces to

$$S^{(\infty)}(\boldsymbol{\rho}, z) = \frac{z_{\mathrm{R}}^2}{z^2} \exp\left(-\frac{z_{\mathrm{R}}^2}{z^2} \frac{2\boldsymbol{\rho}^2}{w_0^2}\right) \left[1 + (-1)^m \cos(m\varphi)\right], \tag{32}$$

which has a periodic azimuthal variation without a quasiperiodic radial dependence. Considering the opposite limit $q \ll 1$, we have

$$S^{(\infty)}(\boldsymbol{\rho}, z) = p_m \frac{z_{\mathrm{R}}^2}{z^2} \exp\left(-\frac{z_{\mathrm{R}}^2}{z^2} \frac{2\boldsymbol{\rho}^2}{w_0^2}\right) \left[1 + C_m (-1)^m \cos(m\varphi) \exp\left(-\frac{R^2}{2}\right) J_m\left(\frac{2R}{q} \frac{z_{\mathrm{R}}}{z} \frac{\rho}{w_0}\right)\right]. \tag{33}$$

In the limit $z/z_{\mathrm{R}} \ll 1$ the underlying GSM beam becomes quasihomogeneous, but the RAP beams considered here do not. The far-zone intensity of any quasihomogeneous field is known to be of the same functional form as the Fourier transform of the source plane DOC, i.e., the function $p(\mathbf{v})$. However, in our case an extra factor $\exp\left(-R^2/2\right)$ appears in front of the Bessel term.

Considering the fundamental $m = 0$ solution, the propagation equations reduce to those of the GSM beam when $C_0 = 1$. When $C_0 = -1$ and the limit $r_0 \to 0$ is considered, they reduce to the expressions for the $n = 1$ LGSM beam [22]. In particular, Eq. (31) takes the form

$$S^{(\infty)}(\boldsymbol{\rho}, z) = \frac{z_{\mathrm{R}}^2}{z^2} \exp\left(-\frac{z_{\mathrm{R}}^2}{z^2} \frac{2\boldsymbol{\rho}^2}{w_0^2}\right) \left(\frac{z_{\mathrm{R}}^2}{z^2} \frac{2\boldsymbol{\rho}^2}{w_0^2} + q^2\right) \left(1 + q^2\right)^{-1}, \tag{34}$$

which is consistent with Eq. (18) of Ref. [8]. This intensity profile approaches a Gaussian shape in the coherent limit $q \to \infty$ and has a flat-top profile (second derivative equal to zero) when $q = 1$. When $q < 1$ it becomes annular with a peak at $\rho_0/w_0 = [(1-q^2)/2]^{1/2} z/z_{\mathrm{R}}$, having an axial dip that approaches zero when $q \to 0$.

4. Source characteristics and beam propagation features

Having mathematically defined the class of quasi RAP sources and derived expressions for propagation of the beams they radiate, we proceed to examine in more detail the optical properties of these sources and beams in terms of the two characteristic ratios r (or R) and q.

Let us first visualize correlations at the source plane by plotting distributions of the complex DOC, $\mu^{(0)}(\Delta\boldsymbol{\rho}')$ in Eqs. (14) and (13), as a function of normalized coordinates $\Delta\boldsymbol{\rho}/\sigma_0$, for some selected values of the parameter r and the index m. Figure 1 displays the $\mu^{(0)}(\Delta\boldsymbol{\rho}')$ for different indices m and a fixed ratio r. The top and bottom rows show the modulus and phase of the DOC, respectively. To visualize the relatively faint side-lobe structure more clearly, we display on the top row the square root of the modulus $\left|\mu^{(0)}(\Delta\boldsymbol{\rho}')\right|$.

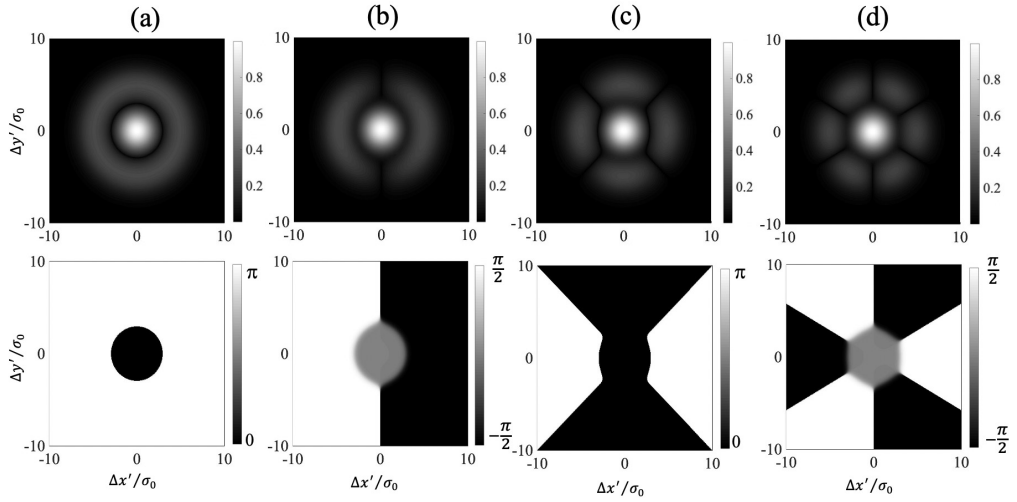

Fig. 1. Source-plane DOC with fixed $r = 5$ for different values of index m: (a) $m = 0$, (b) $m = 1$, (c) $m = 2$, and (d) $m = 3$. The top row shows the square root of the modulus of the DOC, while the bottom row illustrates the phase.

Column (a) in Fig. 1 illustrates the (real-valued) DOC of the fundamental $m = 0$ solution with $C_0 = -1$. The modulus of the DOC has a central lobe with r-dependent width, and a single side lobe with an r-dependent scale. The phase of the DOC is zero within the central peak and π outside it. With $C_0 = 1$, the DOC of the $m = 0$ solution is always real and positive. It is close to Gaussian for small values of r, and the side lobe begins to form clearly when $r > 0$; for values $r \gg 1$ the absolute values of the DOC become identical for both sign choices. Also for $m > 0$, as illustrated in columns (b)–(d) of Fig. 1, there is a clear central lobe and a single side lobe, in which the azimuthal variation caused by the cosine term is clearly visible. The nature of the phase of the DOC depends critically on whether we consider even or odd values of m. For even values the DOC is real and hence the phase is either zero or π. For odd values the phase varies continuously within the interval $[-\pi/2, \pi/2]$, being close to zero within most of the central lobe and transforming into a nearly binary form in the side lobe.

In Fig. 2 we fix the order index m and consider the effect of varying the scale parameter r. Here we concentrate on the (square root of) the modulus of the DOC; the phases (not shown) are again binary for even m and vary continuously for odd n. In the top row we consider the fundamental solution $m = 0$ with $C_0 = 1$. In the limit $r \to 0$ we obtain the LGSM source, for which the radius of the main lobe is at $\rho = \sqrt{2}\sigma_0$, and the peak of the side lobe is located at $\rho = 2\sigma_0$. When r is increased, the scale expands as shown in (a) and (b), and for values $r > 4$ a widening dark annular zone begins to emerge between the bright central lobe and the annular side lobe. The peak radius of the side lobe increases non-linearly, but in the limit $r \gg 1$ we have an asymptotic solution $\rho \to r\sigma_0$. In this limit the width of the central lobes no longer changes appreciably. If the fundamental $m = 0$ solution with $C_0 = 1$ is chosen, a similar dark annulus is formed (though at somewhat larger values of r), and for large r the distributions for both sign choices become the same. Hence, in the limit $r \gg 1$, the DOC shows somewhat peculiar features: on one hand we have high short-range correlations within the main lobe, followed by the dark annulus with a low DOC, and finally some long-range radial correlations appear within the side lobe.

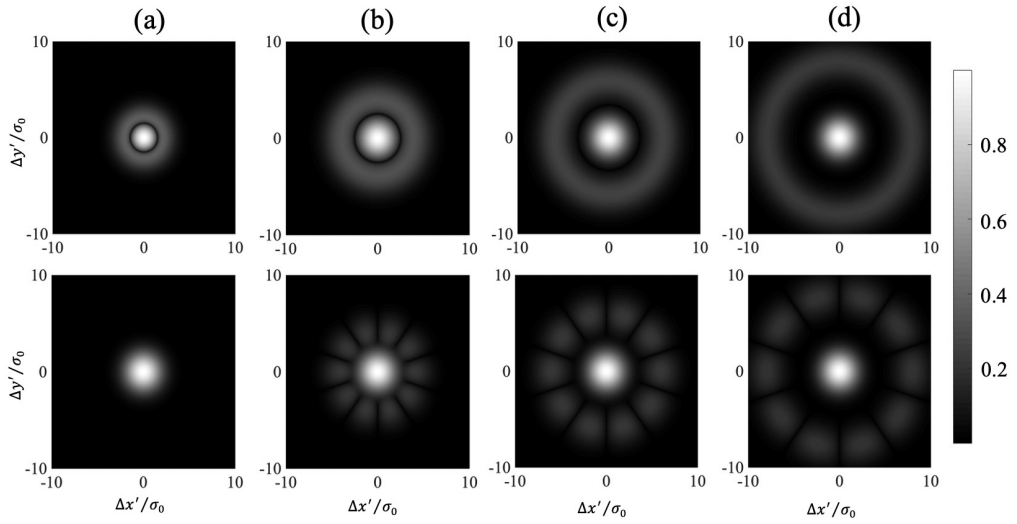

Fig. 2. Square root of the absolute value of the source plane DOC with the index m fixed and r varied: (a) $r = 1$, (b) $r = 4$, (c) $r = 6$, and (d) $r = 8$. Top row: $m = 0$. Bottom row: $m = 5$.

The bottom row in Fig. 2 shows the evolution of the DOC for $m = 5$. For small values of r we have an essentially Gaussian main lobe (irrespective of m). The side lobe, where the azimuthal periodicity can be clearly seen, starts to form at around $r > 2$. Again a dark annulus begins to emerge for $r > 4$ between the nearly rotationally symmetric central lobe and an expanding azimuthally modulated side lobe. Finally, it should be stressed that, even though the side lobe appears dim, it nevertheless has a decisive effect in the properties of the propagated beam.

Let us now proceed to examine the beam properties in the far zone. We found it convenient to use normalized spatial coordinates $\tilde{\boldsymbol{\rho}} = \boldsymbol{\rho} z_{\mathrm{R}}/(z w_0)$ in this zone, and to normalize the spectral density as $\tilde{S}^{(\infty)}(\boldsymbol{\rho}, z) = S^{(\infty)}(\boldsymbol{\rho}, z)\,(z/z_{\mathrm{R}})^2$. With these choices we compare the far-fields of the quasi RAP beams to those of the underlying GSM beam. When considering the modulus $\left|\mu^{(\infty)}(\tilde{\boldsymbol{\rho}}_1, \tilde{\boldsymbol{\rho}}_2, z)\right|$ of the far-zone DOC, we again plot its square root. Finally, when considering the phase $\arg\left[\mu^{(\infty)}(\tilde{\boldsymbol{\rho}}_1, \tilde{\boldsymbol{\rho}}_2, z)\right]$ of the DOC, we plot the residual phase left after the spherical phase in Eq. (29) has been extracted. In plotting results for propagated beams we additionally consider the ratio R instead of r.

It is clear from Eq. (31) that the modulation contrast in the far-zone intensity profiles can be high only if the exponential factor in the Bessel contribution is of the order of unity, which is satisfied (for all values of q) if $R \sim \sqrt{2}$ or smaller. This condition alone ensures the visibility of the azimuthal periodicity. However, to observe radial quasiperiodicity, the first zero $\tilde{\rho}_0^{(m)}$ of the m:th-order Bessel contribution should satisfy (at least) the condition $\tilde{\rho}_0^{(m)} < 1$, which leads to $q < 2R/\tilde{\rho}_0^{(m)}$ if $q \ll 1$. To ensure that the first condition is securely satisfied, we now set $R = 0.5$ and examine the dependence of the far-field beam properties on the global coherence parameter q and the index m.

In Fig. 3 we first consider the case with moderate spatial coherence by fixing $q = 0.1$. At this value of the coherence parameter the azimuthal periodicity of the intensity profile is clearly visible and radial quasiperidicity is emerging. When the value of q is reduced further, to $q = 0.01$, also the radial structure of the beam becomes pronounced. On the other hand, the absolute value of the DOC approaches a Gaussian shape in these two cases. As the DOC takes real values (after spherical phase removal), its phase is not of interest. Therefore, we do not show the properties of DOC here to avoid redundancy.

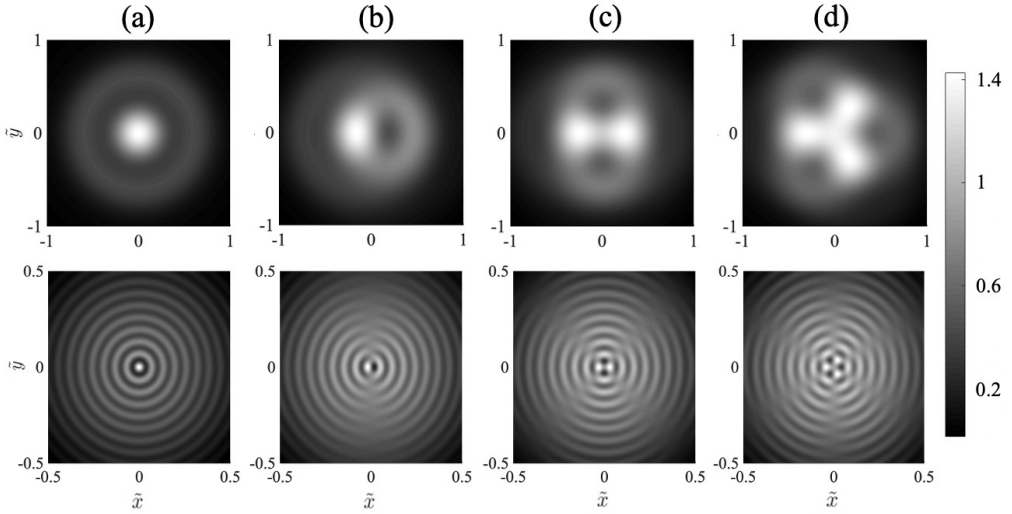

Fig. 3. Far-zone spectral density of the quasi RAP beam with $R = 0.5$, and (a) $m = 0$, (b) $m = 1$, (c) $m = 2$, and (d) $m = 3$. Top row: $q = 0.1$. Bottom row: $q = 0.01$.

When the beam propagates from the source plane towards to far zone, its quasi RAP features emerge gradually. The DOC loses its side-lobe structure and the intensity profile its original Gaussian form, begins to acquire azimuthal periodicity as well as radial quasiperiodicity. These transformations take place at distances of the order of the Rayleigh range of the corresponding GSM beam. In Fig. 4 we illustrate the intensity distributions and the DOC at a propagation distance $z = 3z_{\mathrm{R}}$. The spatial coordinates are scaled to $w(z)$ and the spectral density is also normalized to $(z/z_{\mathrm{R}})^2$. From Fig. 4 we can see that the quasi RAP effect is obvious in the intensity distribution and the DOC, in particular in its phase. The phase distribution, compared to that possessing azimuthal periodicity only in the source plane, exhibits quasi radial periodicity in the outer radial directions after propagation.

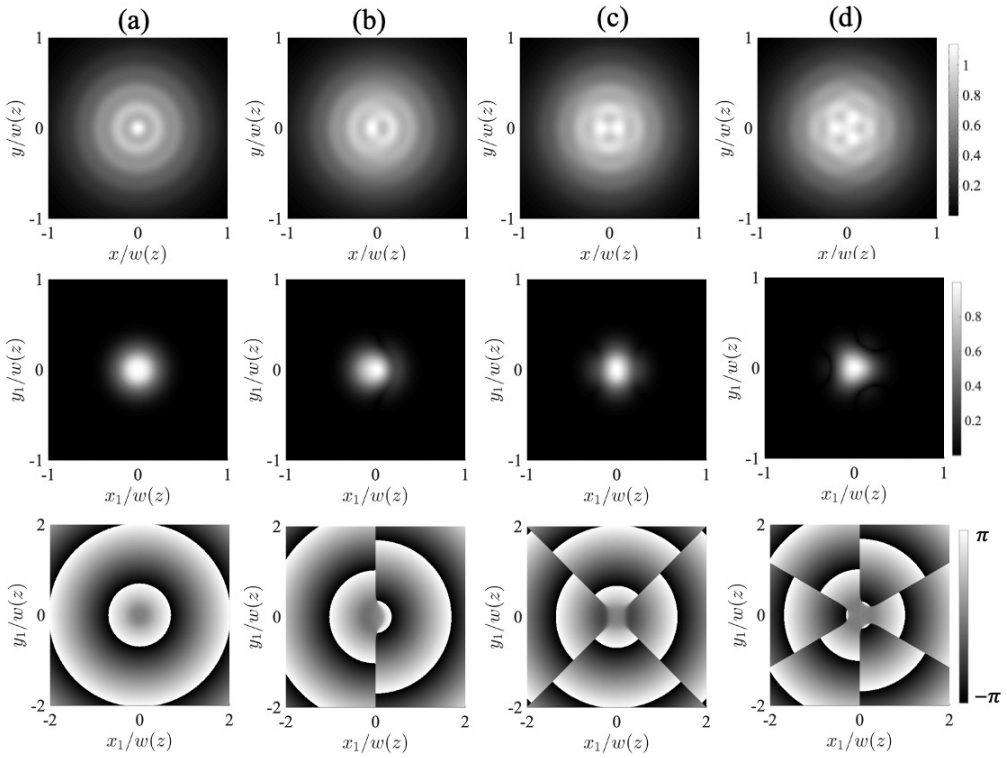

Fig. 4. Spectral density and DOC $\mu(\boldsymbol{\rho}_1, 0, z)$ of the quasi RAP beam in the top row of Fig. 3 ($q = 0.1$) at a propagation distance $z = 3z_{\mathrm{R}}$. Top row: spectral density. Middle row: square root of the modulus of the DOC. Bottom row: residual phase of the DOC.

5. Experimental feasibility

Beams of the type considered here can be generated experimentally along the lines proposed by Gori and Santarsiero [5], in a $2f$ Fourier-transform setup outlined in Fig. 5. The desired source plane CSD, $W^{(0)}(\boldsymbol{\rho}_1', \boldsymbol{\rho}_2')$, is generated at the output plane of the system, behind a Gaussian transmission filter of width w_0, from an incoherent input-plane field with a spatial intensity profile proportional to $p(\boldsymbol{v})$.

In general, one can use spatially uniform incoherent input-plane illumination and modulate the intensity profile with a continuous-tone filter P having a transmittance defined by Eq. (9). However, in our case $p(v, \phi)$ is a product of a radial Gaussian factor and a modulation factor. It is therefore far more light-efficient to first produce the Gaussian profile using an appropriately scaled image (provided by L1) of an incoherent Gaussian field generated, e.g., by illuminating a rotating diffuser RD with a Gaussian laser beam. This leaves only the modulation factor $M(v, \phi) = M_0 \left[1 \pm J_m(2\pi r_0 v)\cos(m\phi)\right]$ to be produced by the intensity filter P. Here M_0 is chosen such that the maximum value of $M(v, \phi)$ does not exceed unity.

The filter P can in principle be produced by techniques such as grey-tone lithography or a grey-tone SLM. However, using spatially variable diffraction gratings is an attractive option. Consider, for instance, a linear binary phase grating of period d, line width c, and a depth corresponding to a phase delay of π radians between the lines and trenches. In view of the standard complex-amplitude transmission approach, the zeroth-order efficiency η_0 of such a grating depends on the fill factor $f = c/d$ according to $\eta_0 = (1 - 2f)^2$.

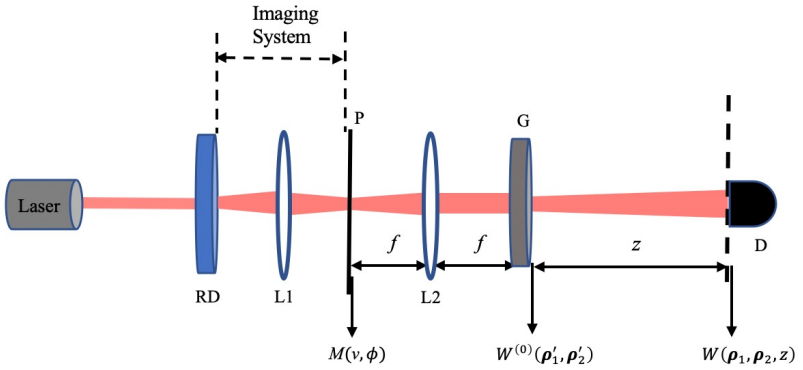

Fig. 5. Schematic setup for experimental generation and characterization of quasi RAP beams: RD is a rotating diffuser, P is an intensity filter, L1 represents an (afocal) imaging system, L2 is a Fourier-transform lens of focal length f, G is a Gaussian transmission filter, and D is a coherence detector.

Hence, if $f = 0$ or $f = 1$ (no grating), all light ends up in the zeroth order, while for other values of f some of the incident light is diffracted into higher orders indexed by an integer $l \neq 0$. In particular, $\eta_0 = 0$ if $f = 1/2$, offering us a possibility to encode the modulation function $M(v, \phi)$ into local fill-factor variations $f(v, \phi)$ of a linear grating. This is accomplished if we demand that

$$[1 - 2f(v, \phi)]^2 = M(v, \phi), \tag{35}$$

which results in a coding

$$f(v, \phi) = \frac{1}{2}\left[1 + \sqrt{M(v, \phi)}\right] \tag{36}$$

of $M(v, \phi)$ into the local fill factor $f(v, \phi)$. The higher orders $l \neq 0$ are (in paraxial approximation) centered at spatial positions $x_l = lf/d$ in the $\boldsymbol{\rho}'$-plane and are therefore filtered out by G if the parameters are chosen such that $|x_{\pm 1}| \gg w_0$. As a result, the grating appears as a metasurface with intensity transmittance $M(v, \phi)$.

We are currently planning an experimental setup of the type just described, with binary-phase grating filters fabricated by electron beam lithography and dry etching, and using a mirror-based wavefront folding interferometer [23] as the coherence (and intensity) detector D in Fig. 5.

6. Conclusions

We have introduced a class of partially coherent sources that radiate quasi RAP intensity patterns as a consequence of a combination of a Bessel function and a cosine function in the source-plane complex DOC. Its primary characteristic is the adjustable periodicity and symmetry. The periodicity in radial direction is governed by the zeros of the derivative of the Bessel function of the first kind, J_m', which is a function of source global coherence length $q = \sigma_0/w_0$ and the radius r_0. The azimuthal periodicity can be modulated by the mode index m. This can be interpreted by the phase discontinuity of the CSD that leads to the periodic changes of the intensity distribution upon propagation. Regarding the symmetry of the intensity patterns, the contribution comes from the model index m. If m is even, the DOC is a real-valued function, and hence, the intensity pattern remains symmetric about the origin. When m takes odd values, indicating that the DOC is a complex function, the field is asymmetric about the origin. The ability of the quasi RAP beam to present peculiar periodic intensity patterns suggests that it may find potential applications in multi particle trapping and optical fractionation procedures.

Appendix

Using the polar representation also for spatial-difference coordinates and the weight function in (9), Eq. (5) takes the form

$$f(\Delta\rho', \Delta\varphi') = 2\pi\sigma_0^2 \int_0^\infty \int_0^{2\pi} \exp\left(-2\pi^2\sigma_0^2 v^2\right) [1 + J_m(2\pi r_0 v)\cos(m\phi)] \times \exp\left[-i2\pi\Delta\rho' v\cos(\phi - \Delta\varphi')\right] v\mathrm{d}v\mathrm{d}\phi. \tag{37}$$

By using the formulas [24]

$$\exp(-ia\cos\theta) = \sum_{n=-\infty}^{\infty} (-i)^n J_n(a)\exp(-in\theta), \tag{38a}$$

$$\int_0^{2\pi} \exp(in\theta)\mathrm{d}\theta = \begin{cases} 2\pi & \text{if } n = 0, \\ 0 & \text{if } n \neq 0, \end{cases} \tag{38b}$$

Eq. (37) becomes

$$f(\Delta\rho', \Delta\varphi') = 2\pi\sigma_0^2 \sum_{n=0,\pm m} (-i)^n \exp(in\Delta\phi)\mathcal{H}_n\left\{t_n \exp\left(-2\pi^2\sigma_0^2 v^2\right)\right\}. \tag{39}$$

Here $t_0 = 1$, $t_{\pm m} = \frac{1}{2}J_m(2\pi r_0 v)$, and $\mathcal{H}_n$ represents the Hankel transform of order n, defined as

$$\mathcal{H}_n\{G(v)\} = 2\pi \int_0^\infty vG(v)J_n(2\pi v\Delta\rho')\mathrm{d}v. \tag{40}$$

Then, by employing the formulas [24]

$$\int_0^\infty x^{m+1} e^{-\alpha x^2} J_m(\beta x)\mathrm{d}x = \frac{\beta^m}{(2\alpha)^{m+1}}\exp\left(-\frac{\beta^2}{4\alpha}\right), \tag{41a}$$

$$\int_0^\infty e^{-\gamma x^2} J_m(\alpha x)J_m(\beta x)x\mathrm{d}x = \frac{1}{2\gamma}\exp\left(-\frac{\alpha^2 + \beta^2}{4\gamma}\right) I_m\left(\frac{\alpha\beta}{2\gamma}\right), \tag{41b}$$

Eq. (39) yields

$$f(\Delta\rho', \Delta\phi') = \exp\left(-\frac{\Delta\rho'^2}{2\sigma_0^2}\right)\left[1 + \cos(m\Delta\varphi')\exp\left(-\frac{r_0^2}{2\sigma_0^2}\right) I_m\left(\frac{r_0\Delta\rho'}{\sigma_0^2}\right)\right]. \tag{42}$$

Since $f(0) = 1$ in Eq. (8), we obtain Eq. (13) in the main text.

Funding

M. Luo acknowledges the financial support of the National Natural Science Foundation of China (NSFC) (61805080), Hunan Provincial Natural Science Foundation of China (2019JJ50366) and the China Scholarship Council (CSC). M. Koivurova and J. Turunen acknowledge the financial support of the Academy of Finland through the PREIN Flagship Programme (projects 320165, 320166), and project 333938.

Disclosures

The authors declare no conflicts of interest.

References

1. L. Wang, C. Zhao, L. Wang, X. Lu, and S. Zhu, "Effect of spatial coherence on radiation forces acting on a Rayleigh dielectric sphere," Opt. Lett. **32**, 1393–1395(2007).
2. J. Kim, D. T. Miller, , E. Kim, S. Oh, J. Oh, and T. E. Milner, "Optical coherence tomography speckle reduction by a partially spatially coherent source," J. Biomed. Opt. **10**, 064034 (2005).
3. G. Gbur and E. Wolf, "Spreading of partially coherent beams in random media," J. Opt. Soc. Am. A **19**, 1592–1598 (2002).
4. A. Starikov and E. Wolf, "Coherent-mode representation of Gaussian Schell-model sources and of their radiation fields," J. Opt. Soc. Am. **72**, 923–928 (1982).
5. F. Gori and M. Santarsiero, "Devising genuine spatial correlation functions," Opt. Lett. **32**, 3531–3533 (2007).
6. F. Gori, V. R. Sanchez, M. Santarsiero, and T. Shirai, "On genuine cross-spectral density matrices," J. Opt. A: Pure Appl. Opt. **11**, 085706 (2009).
7. H. Lajunen and T. Saastamoinen, "Propagation characteristics of partially coherent beams with spatially varying correlations," Opt. Lett. **36**, 4104–4106 (2011).
8. Z. Mei and O. Korotkova, "Random sources generating ring-shaped beams," Opt. Lett. **38**, 91–93 (2013).
9. F. Wang and O. Korotkova, "Random sources for beams with azimuthal intensity variation," Opt. Lett. **41**, 516–519 (2016).
10. M. Luo and D. Zhao, "Elliptical Laguerre Gaussian Schell-model beams with a twist in random media," Opt. Express **27**, 30044–30055 (2019).
11. C. Ding, M. Koivurova, J. Turunen, and L. Pan, "Temporal self-splitting of optical pulses," Phys. Rev. A **97**, 053838 (2018).
12. M. P. MacDonald, G. C. Spalding and K. Dholakia, "Microfluidic sorting in an optical lattice," Nature **426**, 421–424 (2003).
13. V. R. Daria, P. J. Rodrigo and J. Gluckstad, "Dynamic array of dark optical traps," Appl. Phys. Lett. **84**, 323–325 (2004).
14. L. Ma and S. A. Ponomarenko, "Optical coherence gratings and lattices,"Opt. Lett. **39**, 6656–6659 (2014).
15. L. Wan and D. Zhao, "Twisted Gaussian Schell-model array beams," Opt. Lett. **43**, 3554–3557 (2018).
16. Z. Mei and O. Korotkova, "Sources for random arrays with structured complex degree of coherence," Opt. Lett. **43**, 2676–2679 (2018).
17. S. Zhu, J. Wang, X. Liu, Y. Cai and Z. Li, "Generation of arbitrary radially polarized array beams by manipulating correlation structure," Appl. Phys. Lett. **109**, 161904 (2016).
18. Z. Mei and O. Korotkova, "Asymmetric coherence gratings," Opt. Lett. **45**, 1366–1369 (2020).
19. L. Mandel and E. Wolf, *Optical Coherence and Quantum Optics* (Cambridge University, 1995).
20. A. C. Schell, "A technique for the determination of the radiation pattern of a partially coherent aperture," IEEE Trans. Ant. Propag. **AP-15**, 187–188 (1967).
21. A. T. Friberg and R. J. Sudol, "Propagation parameters of Gaussian Schell-model beams," Opt. Commun. **41**, 1075–1087 (1983).
22. Y. Li, "Laguerre–Gaussian functions and generalized formulation of electromagnetic Gaussian Schell-model sources," J. Opt. Soc. Am. A **32**, 877–885 (2015).
23. A. Halder, H. Partanen, A. Leinonen, M. Koivurova, T. K. Hakala, T. Setälä, J. Turunen, and A. T. Friberg, "Mirror-based scanning wavefront-folding interferometer for coherence measurements, Opt. Lett. **45**, 4260–4263 (2020).
24. I. S. Gradshteyn and I. M. Ryzhik, *Table of Integrals, Series and Products* (Academic, 2007).